THE JOURNAL OF PHYSICAL CHEMISTRY C

ARTICLE

pubs.acs.org/JPCC

Designing All-Graphene Nanojunctions by Covalent Functionalization

Caterina Cocchi,*[,†,‡] Alice Ruini,[†,‡] Deborah Prezzi,[†] Marilia J. Caldas,[§] and Elisa Molinari[†,‡]

[†]Centro S3, CNR-Istituto Nanoscienze, I-41125 Modena, Italy

[‡]Dipartimento di Fisica, Università di Modena e Reggio Emilia, I-41125 Modena, Italy

[§]Instituto de Física, Universidade de São Paulo, 05508-900 São Paulo, SP, Brazil

ABSTRACT: We investigated theoretically the effect of covalent edge functionalization, with organic functional groups, on the electronic properties of graphene nanostructures and nanojunctions. Our analysis shows that functionalization can be designed to tune electron affinities and ionization potentials of graphene flakes, and to control the energy alignment of frontier orbitals in nanometer-wide graphene junctions. The stability of the proposed mechanism is discussed with respect to the functional groups, their number as well as the width of graphene nanostructures. The results of our work indicate that different level alignments can be obtained and engineered in order to realize stable all-graphene nanodevices.

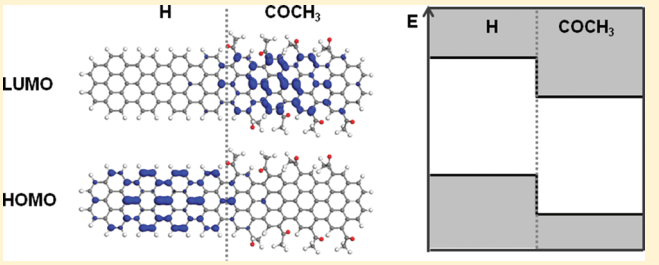

The successful fabrication of the 2D system graphene[1] and its excellent mechanical and electronic properties have aroused great interest in several different fields, both from fundamental research and for technological applications.[2−5] Quasi-1D graphene nanoribbons (GNRs) with semiconducting behavior can also be obtained,[6,7] with electrical band gap tunable within a wide range,[8,9] and their optical properties, even if less intensively studied, offer stimulating perspectives.[10−13] One main challenge is to gain control of the graphene edge morphology at the nanoscale, in view of designing all-graphene nanodevices. In this sense, many recent improvements in production techniques were reported, including both top-down[14−21] and bottom-up[22,23] approaches, which point to the possibility of exploiting the exceptional properties of graphene nanostructures in actual devices (e.g., refs 24−26).

In view of electronic and optoelectronic applications, it is important to identify further approaches for an efficient engineering of the electronic states of a graphene nanostructure. It has recently been shown that the electronic properties of graphene-based systems can be conveniently modulated by means of organic functionalization.[27−30] Until now, a number of procedures have been proposed exploiting either surface functionalization through chemisorption of molecules,[31−33] which is expected however to damage the transport properties of the system, or noncovalent interaction,[34−37] which usually induces doping effects but does not lead to stable structures. A more effective strategy could be edge functionalization,[38,39] which may offer promising perspectives also insofar unexplored application fields, such as the production of GNR-based nanojunctions.

In semiconductor physics, heterojunctions are usually classified on the basis of the relative alignment of valence and conduction band states at the interface of the two materials. Heterostructures where the band gap of one semiconductor is fully contained in the gap of the other are commonly indicated as *type I* or *straddling*. The so-called *type II* or *staggered* alignment is achieved when the top of the valence band and the bottom of the conduction band of one semiconductor are both higher in energy compared to the corresponding states of the other, so that the top of the valence band of the junction lies on one side of the interface, and the bottom of conduction on the other side. In this case, electrons and holes on the frontier orbitals are spatially separated, being located on opposite sides of the junction, which may promote relevant processes, such as for example photoinduced charge separation, as requested by light harvesting applications or photocatalysis. These concepts can be extended to graphene nanojunctions, where the seamless covalent transition from two graphene nanostructures with different electronic characteristics can create, as in conventional semiconductor heterojunctions, different kinds of alignments. Indeed, interfacing semiconducting GNRs with different widths, and consequently different energy gaps, provides a *type I* level line-up.[12,40] In this article, we propose a proof of concept for a viable method to realize all-graphene *type II* nanojunctions. For this purpose, we investigate the effects of stable edge functionalization through organic electron-donating and electron-withdrawing groups, which modify electron affinities and ionization potentials in comparison with the H-terminated GNR. The proposed model for chemical engineering carries a high potential for producing stable graphene nanostructures, preserving their flexibility and

Received: October 15, 2010
Revised: December 13, 2010
Published: February 3, 2011

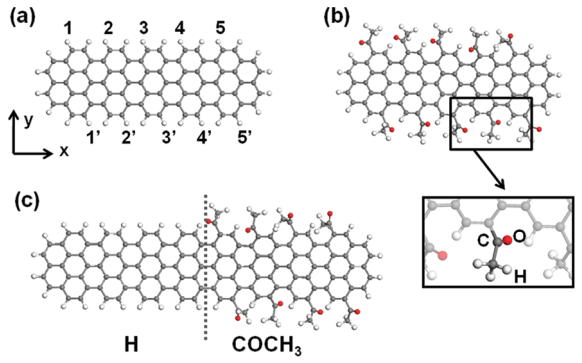

Figure 1. (Color online) (a) Hydrogenated $C_{80}H_{28}$ graphene nanoflake (GNF); the numbers identify the hydrogen atoms that can be substituted by the organic groups upon functionalization. (b) Fully functionalized GNF obtained by replacing each second H atom terminating the edge [i.e., 1−5 and 1′−5′ in panel (a)] with a $-COCH_3$ radical; in the insert, the atoms of the radical are highlighted. (c) Nanojunction obtained by fully functionalizing one side of a $C_{122}H_{40}$ GNF with $-COCH_3$ groups.

their intrinsic electronic features, sp^2 carbon network being unaltered upon functionalization.

METHODS

As prototypes for graphene nanoribbons we consider sub-nanometer-wide graphene nanoflakes (GNFs), that is, finite systems, and we focus in particular on H-terminated GNFs (part a of Figure 1), organically functionalized GNFs (part b of Figure 1), as well as on the nanojunction obtained by functionalizing one-half of the flake with $-COCH_3$ groups (part c of Figure 1). In this case, we will be interested in the frontier molecular orbitals (that stand here for the conduction and valence band states) and their localization and energy alignment across the differently terminated regions. To have access to the electronic energies, we performed calculations in the frame of the semiempirical AM1 scheme.[41,42] AM1 is a well tested method based on the Hartree−Fock scheme,[43] suitable for finite structures;[44−50] it allows one to evaluate the ground state properties of the system and to compute the electrical band gap E_G as the difference between electron affinity (EA) and ionization potential (IP). The latter quantities are expressed in terms of the total energy of the neutral $[E(0)]$ and charged systems $[E(\pm1)]$, in the usual way EA = $E(0) - E(-1)$ and IP = $E(+1) - E(0)$. For all the considered structures, we performed full geometrical optimization to evaluate $E(0)$, with a threshold for the forces of 0.4 kcal·mol^{-1}/Å. The $E(\pm1)$ are obtained at the fixed atomic positions optimized in the ground state, that is *vertical* EA and IP are computed.

RESULTS AND DISCUSSION

Our reference system is the $C_{80}H_{28}$ flake (part a of Figure 1), characterized by armchair-shaped H-saturated edges along the length (x direction in Figure 1). We checked that the chosen length/width ratio is such that the zigzag-shaped end-borders (y direction) do not affect the intrinsic properties related to the armchair edges along the length. Thus, $C_{80}H_{28}$ is a suitable model for an armchair GNR of width parameter $N = 7$, N being the number of dimer lines across the ribbon width, according to the standard notation.[8] It corresponds to an effective width of ∼7 Å, defined as the distance between C atoms on opposite edges, belonging to the same zigzag chain along y. Next, we addressed the same GNF upon covalent edge functionalization with organic groups. We started focusing on molecules containing a ketone functional group, characterized by high electronegativity of its carbonyl oxygen atoms, and in particular we considered the methyl ketone group $-COCH_3$ (insert in part b of Figure 1), which is known to be more stable than the simpler formaldehyde group −COH. We simulated full functionalization of the $C_{80}H_{28}$ by replacing each second H atom along the length with methyl ketone, corresponding in this case to ten anchored groups per flake $[C_{80}H_{18}(COCH_3)_{10}]$, that is five per edge side, as shown in part b of Figure 1. We computed E_G, EA, and IP, and we compared these quantities to those evaluated for $C_{80}H_{28}$ by calculating ΔEA (ΔIP) as the difference between EA (IP) of the functionalized and hydrogenated GNF, respectively. A positive shift of both EA and IP is revealed, as shown in the second column of Table 1.

In addition to the methyl ketone group, we considered the case of other organic functionalizations. We focused on few prototypical substituents, such as (i) a methoxy group ($-OCH_3$), characterized by an O-bridge ester bond, which is known to be electron-donating with respect to aromatic molecules;[51] (ii) a $-CH{=}CF_2$ group, which is expected to be electron-withdrawing, due to the high electronegativity of its F-termination; (iii) a $-OCF{=}CF_2$ group, which combines the presence of O-bridge ester bond and halogen termination. Because of their characteristics, we expect group (i) to provide a similar effect compared to methyl ketone, that is to rise EA and IP with respect to the hydrogenated flake, and group (ii) to do the opposite. In the case of $-OCF{=}CF_2$, the coexistence of both O-bridge bond and F-termination makes the picture less predictable. We also consider $-CH{=}CH_2$ and $-(CH)_3{=}CH_2$ functionalizations, which do not introduce any foreign species in the system and preserve its C−sp^2 conjugation through the alternation of single and double C−C bonds. For each chosen group we addressed full functionalization, analogously to the case of $-COCH_3$ illustrated in part b of Figure 1, and we computed E_G, EA, and IP.

By inspecting the complete results in Table 1, two main features arise. The first is related to a decrease of the energy gap, independently of the anchored group: this is ascribed to an increase of the effective width of the flake, compared to the fully hydrogenated case. The other important outcome concerns the sign of ΔEA and ΔIP: we observe positive (negative) values of both ΔEA and ΔIP, corresponding to a downshift (upshift) of both HOMO and LUMO for groups with a predominant electron-withdrawing (-donating) character, as well as for $-OCF{=}CF_2$. On the contrary, $-CH{=}CH_2$ and $-(CH)_3{=}CH_2$ functionalizations produce ΔEA and ΔIP having opposite signs: given the simple bond-alternating character of the functional group, the major result is related to the extension of the wave function to a larger effective width, which thus reduces E_G in agreement with results for 1D GNRs.[12]

The analysis of Mulliken charge population shows that a charge redistribution at the edge occurs upon functionalization. In particular, Mulliken charges of functionalized C edge atoms become more positive, being these atoms bonded to more electronegative species than H. Larger differences (>0.2 e^-) are observed when functional groups are bonded to the flake through an O-bridge ester bond, that is $-OCH_3$ and $-OCF{=}CF_2$. Moieties bonded through C atoms induce slighter Mulliken charge redistribution, of the order or less than 0.1 e^-. It is important to highlight that these redistribution effects vanish within one aromatic ring.

Table 1. (Color Online) Energy Gap (E_G) and Variations in EA and IP (ΔEA and ΔIP), Computed with Respect to the Reference Hydrogenated $C_{80}H_{28}$ (H), of GNFs Fully Functionalized with Different Organic Groups[a]

	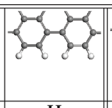	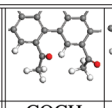	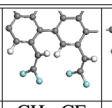	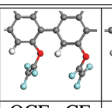	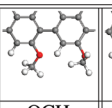	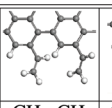	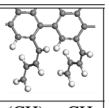
	H	-$COCH_3$	-$CH{=}CF_2$	-$OCF{=}CF_2$	-OCH_3	-$CH{=}CH_2$	-$(CH)_3{=}CH_2$
E_G [eV]	5.13	4.86	4.65	4.74	4.75	4.76	4.67
ΔEA [eV]	0.00	0.69	0.67	0.70	-0.12	0.14	0.15
ΔIP [eV]	0.00	0.42	0.19	0.31	-0.50	-0.22	-0.31

[a] Among the considered groups, $-COCH_3$, $-CH{=}CF_2$, $-OCF{=}CF_2$, and $-OCH_3$ give rise to a *type II* offset, with a positive (negative) sign of ΔEA and ΔIP for electron-withdrawing (-donating) groups; $-CH{=}CH_2$ and $-(CH)_3{=}CH_2$ produce a *type I* offset.

Table 2. Energy Gap (E_G) and Variations in EA and IP (ΔEA and ΔIP) of the GNF Functionalized with an Increasing Number of $-COCH_3$ Groups, up to 10 (Full Functionalization), with Respect to Hydrogenated $C_{80}H_{28}$ (H)

	H	2	4	6	8	10
E_G [eV]	5.13	5.01	5.01	4.99	4.96	4.86
ΔEA [eV]	0.00	0.21	0.29	0.37	0.47	0.69
ΔIP [eV]	0.00	0.09	0.17	0.23	0.30	0.42

We also performed some tests on functionalized $C_{80}H_{28}$ at decreasing number of functional groups (Table 2). We focus here on $-COCH_3$ as an illustrative example but this behavior is independent of the anchored group. We take the hydrogenated flake and, retaining the symmetry of the system, we introduce increasing even numbers of functional groups, up to 10, which corresponds to full functionalization for the chosen $C_{80}H_{28}$ flake (part b of Figure 1). We start from two anchored groups in positions 3 and 3′, after the scheme in part a of Figure 1, which corresponds to a $-COCH_3$ substituent each fifth H atom. We then introduce four and six groups in positions (2, 2′, 4, 4′) and (1, 1′, 3, 3′, 5, 5′), respectively. In the case of eight bonded groups, to maintain the symmetry of the graphene flake, each H atom in positions (1, 1′, 2, 2′, 4, 4′, 5, 5) is replaced by a $-COCH_3$. The results, reported in Table 2, show a monotonic growth of both ΔEA and ΔIP with increasing number of covalently bonded groups, with an almost linear dependence for ΔIP. At the same time, we notice the monotonic decrease of E_G, consistent with the above-mentioned picture related to the increased effective width of the GNF.

We also discuss the dependence of the electronic properties of the GNF, specifically related to EA and IP, by directly increasing its width. For this purpose, we performed a systematic investigation on GNFs, characterized by fixed length (along the *x* direction in Figure 1) and increasing width (along the *y* direction), fully functionalized with 16 $-COCH_3$ groups.[52] We studied 8 GNFs ranging from width parameter $N = 4$ (less than 4 Å wide) to $N = 11$ (about 12 Å wide) and we computed EA and IP for each of them. As shown in Figure 2, the calculated values for EA and IP have an oscillating behavior characterized by the *modulo* 3 periodicity already encountered in infinite GNRs,[8,53,54] with the smallest value of the energy gap pertaining to the $N = 3p + 2$ family (p integer). An approximate $\sim 1/w$ dependence (being w the GNF width) is recognizable for the energy gap, consistently with well-known theoretical[8,9] and experimental[6,7] results. The values of ΔEA and ΔIP, represented in Figure 2 by

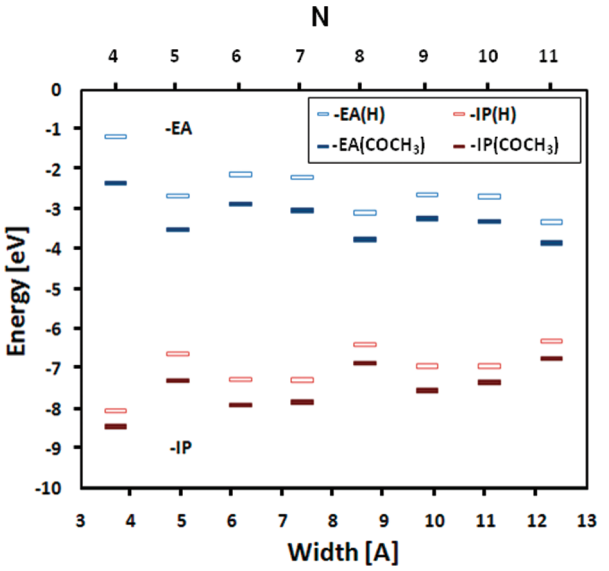

Figure 2. (Color online) Negative of electron affinity and ionization potential (−EA and −IP, respectively) of hydrogenated (H) and ($-COCH_3$) functionalized GNFs of increasing width. We also indicate the parameter *N*, i.e. the number of C−C dimers along the width.

the spacing between the respective marks, show a faster decay, which may be compatible with a local dipole mechanism driving the offset between functionalized and hydrogenated flakes. For instance, for the $3p + 2$ family, we get values of ΔEA = 0.85 eV and ΔIP = 0.67 eV for the smallest computed flake ($N = 5$, w = 4.9 Å) and ΔEA = 0.53 eV and ΔIP = 0.43 eV for the largest one ($N = 11$, w = 12.3 Å). From the results in Figure 2, we can extrapolate non-negligible effects of covalent functionalization also for nanometer-sized graphene flakes, which can be considered realistic for current nanofabrication approaches.

Finally, we directly investigate the *type II* nanojunction obtained by connecting a fully hydrogenated GNF to a fully functionalized one, having the same width (part c of Figure 1). For this purpose, we adopted a flake of the same width of $C_{80}H_{28}$ but increased global length to ensure that each side of the junction is long enough to confidently reproduce the *bulk* properties of the flake (i.e., same single-particle orbitals in the energy range close to the energy gap). The resulting system accommodates full functionalization of one-half flake with eight radicals, four per side (part c of Figure 1). We first performed full geometrical optimization and then focused on the ground state electronic properties of the junction. In particular, we are interested in the energy and wave function localization of the

dx.doi.org/10.1021/jp109909s |J. Phys. Chem. C 2011, 115, 2969–2973

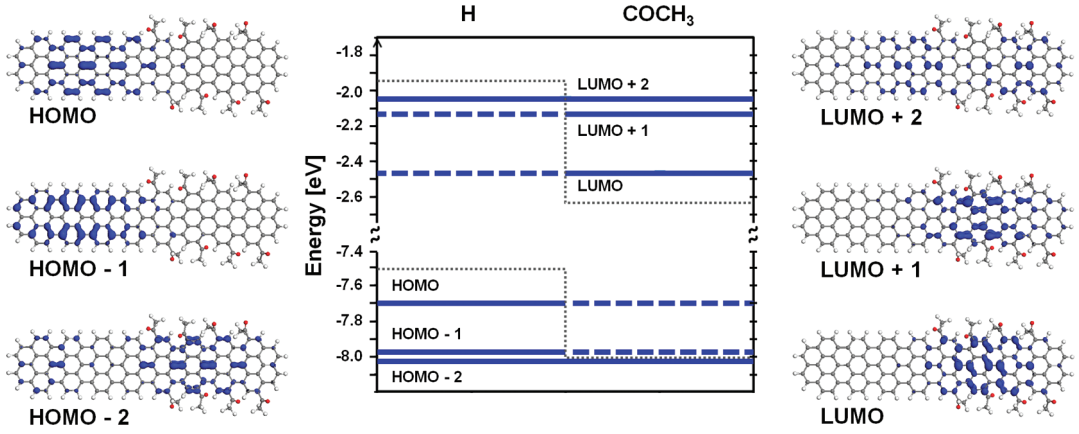

Figure 3. (Color online) Energy levels (center) and wave function distributions (sides) of the frontier states of the nanojunction (part c of Figure 1). The dotted gray line in the energy level diagram indicates the reference (from the homogeneous GNFs) for HOMO and LUMO of the hydrogenated (H) and functionalized ($-COCH_3$) sides of the GNF. The energy positions of the six frontier orbitals represented at the side panels are marked by the heavier (blue) lines: the solid intervals indicate finite wave function probability, whereas dashed intervals indicate vanishing wave function probability.

frontier states, as summarized in Figure 3. The analysis of the wave function distributions clearly reflects the *type II* character of this junction. In fact, we observe that the top valence states, HOMO and HOMO−1, are localized on the hydrogenated side of the junction, while the bottom conduction states, LUMO and LUMO+1, are localized on the functionalized side. However, the next states HOMO−2 and LUMO+2 show already resonant character. This feature can be explained in terms of the absolute energy levels of the *bulk* of the two sides, as indicated in the graph of Figure 3: we represent by the dotted gray line the gap of the homogeneous systems, hydrogenated and functionalized, evaluated from the HOMO and LUMO levels of the fully hydrogenated $[C_{116}H_{40}]$ and functionalized $[C_{116}H_{24}(COCH_3)_{16}]$ GNFs. On top of this we plot the level spectrum for the junction-GNF, highlighting the localization character of the related state through blue solid (finite probability) or dashed (zero probability) lines. We see that HOMO and HOMO−1 lie in the forbidden gap for the functionalized side and are consistently localized on the allowed hydrogenated half; the opposite applies to LUMO and LUMO+1, which are thus localized on the functionalized part. Whereas the numbers for IP and EA in Table 2 are taken from total energy calculations, therefore giving us good precision, we remark that the energy level spectrum shown here is by construction based on one-electron mean-field approximation and cannot give us a level-by-level accuracy, in particular for the unoccupied states. We see however that the overall picture is totally consistent with the *type II* alignment.

CONCLUSIONS

In conclusion, we have studied the effects of organic covalent functionalization on subnanometer sized graphene nanoflakes by varying the anchored groups, the number of functionalizing groups, and the flake width. Our results indicate that edge functionalization can be designed to tune the electronic properties of graphene nanostructures and to control band alignment in graphene nanojunctions while preserving stability and intrinsic electronic properties. This opens the possibility to realize stable all-graphene electronic and optoelectronic nanodevices based on *type II* offset.[55]

AUTHOR INFORMATION

Corresponding Author

*E-mail: caterina.cocchi@unimore.it.

ACKNOWLEDGMENT

The authors acknowledge CINECA for computational support and Stefano Corni and Enrico Benassi for helpful discussions. This work was partly supported by "Fondazione Cassa di Risparmio di Modena", by the Italian Ministry of Foreign Affairs (Italy-USA bilateral project) and by the Italian Ministry of University and Research under FIRB grant ItalNanoNet. M.J.C. acknowledges support from FAPESP and CNPq (Brazil).

REFERENCES

(1) Novoselov, K. S.; Geim, A. K.; Morozov, S. V.; Jiang, D.; Zhang, Y.; Dubonos, S. V.; Grigorieva, I. V.; Firsov, A. A. *Science* **2004**, *306*, 666–669.
(2) Soldano, C.; Mahmood, A.; Dujardin, E. *Carbon* **2010**, *48*, 2127–2150.
(3) Geim, A. *Science* **2009**, *324*, 1530.
(4) Burghard, M.; Klauk, H.; Kern, K. *Adv. Mater.* **2009**, *21*, 2586–2600.
(5) Castro Neto, A. H.; Guinea, F.; Peres, N. M. R.; Novoselov, K. S.; Geim, A. K. *Rev. Mod. Phys.* **2009**, *81*, 109–162.
(6) Han, M. Y.; Ozyilmaz, B.; Zhang, Y.; Kim, P. *Phys. Rev. Lett.* **2007**, *98*, 206805.
(7) Chen, Z.; Lin, Y.-M.; Rooks, M. J.; Avouris, P. *Physica E* **2007**, *40*, 228–232.
(8) Son, Y.-W.; Cohen, M. L.; Louie, S. G. *Phys. Rev. Lett.* **2006**, *97*, 216803.
(9) Yang, L.; Park, C.-H.; Son, Y.-W.; Cohen, M. L.; Louie, S. G. *Phys. Rev. Lett.* **2007**, *99*, 186801.
(10) Prezzi, D.; Varsano, D.; Ruini, A.; Marini, A.; Molinari, E. *Phys. Rev. B* **2008**, *77*, 041404(R).
(11) Prezzi, D.; Varsano, D.; Ruini, A.; Marini, A.; Molinari, E. *Phys. Status Solidi B* **2007**, *244*, 4124–4128.
(12) Prezzi, D.; Varsano, D.; Ruini, A.; Molinari, E. Submitted, 2010.
(13) Yang, L.; Cohen, M.; Louie, S. *Nano Lett.* **2007**, *7*, 3112–3115.
(14) Datta, S. S.; Strachan, D. R.; Khamis, S. M.; Johnson, A. T. C. *Nano Lett.* **2008**, *8*, 1912–1915.
(15) Campos, L. C.; Manfrinato, V. R.; Sanchez-Yamagishi, J. D.; Kong, J.; Jarillo-Herrero, P. *Nano Lett.* **2009**, *9*, 2600–2604.
(16) Li, X.; Wang, X.; Zhang, L.; Lee, S.; Dai, H. *Science* **2008**, *319*, 1229–1232.
(17) Wang, X.; Dai, H. *Nature Chem.* **2010**, *2*, 661–665.
(18) Jia, X.; Hofmann, M.; Meunier, V.; Sumpter, B.; Campos-Delgado, J.; Romo-Herrera, J.; Son, H.; Hsieh, Y.-P.; Reina, A.; Kong, J.; Terrones, M.; Dresselhaus, M. *Science* **2009**, *323*, 1701.

(19) Kosynkin, D. V.; Higginbotham, A. L.; Sinitskii, A.; Lomeda, J. R.; Dimiev, A.; Price, B. K.; Tour, J. M. *Nature (London)* **2009**, *458*, 872.
(20) Jiao, L.; Zhang, L.; Wang, X.; Diankov, G.; Dai, H. *Nature (London)* **2009**, *458*, 877.
(21) Cano-Márquez, A. G.; Rodríguez-Macías, F. J.; Campos-Delgado, J.; Espinosa-González, C. G.; Tristán-López, F.; Ramírez-González, D.; Cullen, D. A.; Smith, D. J.; Terrones, M.; Vega-Cantú, Y. I. *Nano Lett.* **2009**, *9*, 1527.
(22) Yang, X.; Dou, X.; Rouhanipour, A.; Zhi, L.; Rader, H. J.; Muellen, K. *J. Am. Chem. Soc.* **2008**, *130*, 4216.
(23) Cai, J.; Ruffieux, P.; Jaafar, R.; Bieri, M.; Braun, T.; Blankenburg, S.; Muoth, Matthiasand Seitsonen, A. P.; Saleh, M.; Feng, X.; Muellen, K.; Fasel, R. *Nature (London)* **2010**, *466*, 470–473.
(24) Wang, X.; Ouyang, Y.; Li, X.; Wang, H.; Guo, J.; Dai, H. *Phys. Rev. Lett.* **2008**, *100*, 206803.
(25) Xia, F.; Mueller, T.; Lin, Y.; Valdes-Garcia, A.; Avouris, P. *Nature Nanotechnol.* **2009**, *4*, 839–843.
(26) Ponomarenko, L.; Schedin, F.; Katsnelson, M.; Yang, R.; Hill, E.; Novoselov, K.; Geim, A. *Science* **2008**, *320*, 356.
(27) Loh, K.; Bao, Q.; Ang, P.; Yang, J. *J. Mater. Chem.* **2010**, *20*, 2277–2289.
(28) Farmer, D. B.; Golizadeh-Mojarad, R.; Perebeinos, V.; Lin, Y.-M.; Tulevski, G. S.; Tsang, J. C.; Avouris, P. *Nano Lett.* **2009**, *9*, 388–392.
(29) Farmer, D. B.; Lin, Y.-M.; Afzali-Ardakani, A.; Avouris, P. *Appl. Phys. Lett.* **2009**, *94*, 213106.
(30) Lohmann, T.; von Klitzing, K.; Smet, J. *Nano Lett.* **2009**, *9*, 1973–1979.
(31) Lopez-Bezanilla, A.; Triozon, F.; Roche, S. *Nano Lett.* **2009**, *9*, 2537.
(32) Bekyarova, E.; Itkis, M.; Ramesh, P.; Berger, C.; Sprinkle, M.; de Heer, W.; Haddon, R. *J. Am. Chem. Soc.* **2009**, *131*, 1336–1337.
(33) Sinitskii, A.; Dimiev, A.; Corley, D.; Fursina, A.; Kosynkin, D.; Tour, J. *ACS Nano* **2010**, *4*, 1949–1954.
(34) Chen, W.; Chen, S.; Qi, D. C.; Gao, X. Y.; Wee, A. T. S. *J. Am. Chem. Soc.* **2007**, *129*, 10418–10422.
(35) Lu, Y. H.; Chen, W.; Feng, Y. P.; He, P. M. *J. Phys. Chem. B* **2009**, *113*, 2–5.
(36) Zhang, Y.-H.; Zhou, K.-G.; Xie, K.-F.; Zeng, J.; Zhang, H.-L.; Peng, Y. *Nanotechnol.* **2010**, *21*, 065201.
(37) Sun, J. T.; Lu, Y. H.; Chen, W.; Feng, Y. P.; Wee, A. T. S. *Phys. Rev. B* **2010**, *81*, 155403.
(38) Qian, H.; Negri, F.; Wang, C.; Wang, Z. *J. Am. Chem. Soc.* **2008**, *130*, 17970.
(39) Wang, X.; Li, X.; Zhang, L.; Yoon, Y.; Weber, P. K.; Wang, H.; Guo, J.; Dai, H. *Science* **2009**, *324*, 768–771.
(40) Sevinçli, H.; Topsakal, M.; Ciraci, S. *Phys. Rev. B* **2008**, *78*, 245402.
(41) Dewar, M. J. S.; Zoebish, E. G.; Healy, E. F.; Stewart, J. J. P. *J. Am. Chem. Soc.* **1985**, *107*, 3902–3909.
(42) We used AM1 as implemented in the VAMP package, included in *Accelrys Materials Studio* software, version 5.0. See also: http://accelrys.com/products/materials-studio.
(43) Roothaan, C. C. J. *Rev. Mod. Phys.* **1951**, *23*, 69.
(44) Caldas, M. J.; Pettenati, E.; Goldoni, G.; Molinari, E. *Appl. Phys. Lett.* **2001**, *79*, 2505–2507.
(45) Dávila, L. Y. A.; Caldas, M. J. *J. Comput. Chem.* **2002**, *23*, 1135.
(46) Lair, S.; Herndon, W.; Murr, L. *Carbon* **2008**, *46*, 2083–2095.
(47) Tachikawa, H. *J. Phys. Chem. C* **2008**, *112*, 10193–10199.
(48) Hantal, G.; Picaud, S.; Collignon, B.; Hoang, P. N. M.; Rayez, M. T.; Rayez, J. C. *Mol. Simul.* **2009**, *35*, 1130.
(49) Abe, S.; Nagoya, Y.; Watari, F.; Tachikawa, H. *Jpn. J. Appl. Phys.* **2010**, *49*, 01AH07.
(50) Wetmore, S. D.; Boyd, R. J.; Eriksson, L. A. *Chem. Phys. Lett.* **2000**, *322*, 129–135.
(51) Venkataraman, L.; Park, Y.; Whalley, A.; Nuckolls, C.; Hybertsen, M.; Steigerwald, M. *Nano Lett.* **2007**, *7*, 502–506.
(52) To keep an appropriate length/width ratio for all structures, we considered a class of flakes having the same length of the nanojunction (part c of Figure 1).
(53) Nakada, K.; Fujita, M.; Dresselhaus, G.; Dresselhaus, M. S. *Phys. Rev. B* **1996**, *54*, 17954–17961.
(54) Barone, V.; Hod, O.; Scuseria, G. E. *Nano Lett.* **2006**, *6*, 2748–2754.
(55) Cocchi, C.; Prezzi, D.; Ruini, A.; Caldas, M. J; Molinari, E. In preparation, 2010.